Available online at www.sciencedirect.com
SCIENCE DIRECT®
Computer Vision and Image Understanding 101 (2006) 65–86
Computer Vision and Image Understanding
www.elsevier.com/locate/cviu

A paintbrush laser range scanner

Lyubomir Zagorchev, Ardeshir Goshtasby *

Computer Science and Engineering Department, Wright State University, Dayton, OH 45435, USA

Received 7 June 2004; accepted 15 July 2005
Available online 3 October 2005

Abstract

A new hand-held laser range scanner is introduced that can capture multi-view range images of an object and integrate the images without registering them. The scanner uses a reference double-frame that acts as the coordinate system of the object. Range images captured from different views of the object are in the coordinate system of the double-frame and, thus, automatically come together. A single-view image is obtained by sweeping a laser line over the object while keeping the camera fixed and analyzing the acquired laser stripes. The laser line generator and the camera can move independently, making it possible to conveniently scan an object just like painting over it with a paintbrush while viewing it from different views. The hardware and software organization of the scanner are described, the characteristics of the scanner are investigated, and example images captured by the scanner are presented.
© 2005 Elsevier Inc. All rights reserved.

Keywords: Laser range scanner; 3-D scanner; Hand-held scanner; Object-centered scanning; Image integration

1. Introduction

Determination of the 3-D geometry of an object from its images is a fundamental problem in computer vision. Methods for 3-D recovery can be classified into passive and active. Passive methods, such as binocular stereo [38,44,47] and depth from defocus [41,48], use a scene's own lighting, while active techniques, such as structured light [3,28], Moiré interferometry [15,25], and time of flight [46], use special lighting or signal to recover 3-D. In this paper, development of a range scanner based on the structured light principle is described.

Recovery of 3-D information from structured light is based on the triangulation principle depicted in Fig. 1. The intersection of a sheet of light with an object appears as a light stripe in an image of the object. Assuming that the distance d between the light source and the camera and the orientation α of the plane of laser with the baseline (line AB) are known, the angle β between the ray from the object to the camera (line CB) and the baseline is determined by connecting the lens center to the image of point C in the image plane. Therefore, in triangle ABC, by knowing distance d and angles α and β, the distance of point C in the scene to the baseline can be determined. The triangulation angle γ determines the depth resolution. When this angle is small, the depth resolution will be small also. When this angle is zero, objects at different depths cannot be distinguished from each other. As this angle is increased, depth resolution will increase also, enabling a more accurate measurement of depth. Increasing the triangulation angle will increase the depth accuracy, but that will increase the number of holes in captured range images also.

Range scanners determine the coordinates of object points with respect to a coordinate system that is attached to the scanner. To integrate range images captured from different views of an object, transformation functions that contain information about the positions and orientations of the scanner capturing the images are needed. The parameters of the transformation functions can be computed by registering the images. Although registration methods have been developed that can find transformations between a large number of views [30,34], registration is generally a very time consuming process and there is a need to remove it from the range data integration process.

* Corresponding author.
E-mail addresses: lzagorch@cs.wright.edu (L. Zagorchev), ardy@cs.wright.edu (A. Goshtasby).

1077-3142/$ - see front matter © 2005 Elsevier Inc. All rights reserved.
doi:10.1016/j.cviu.2005.07.003

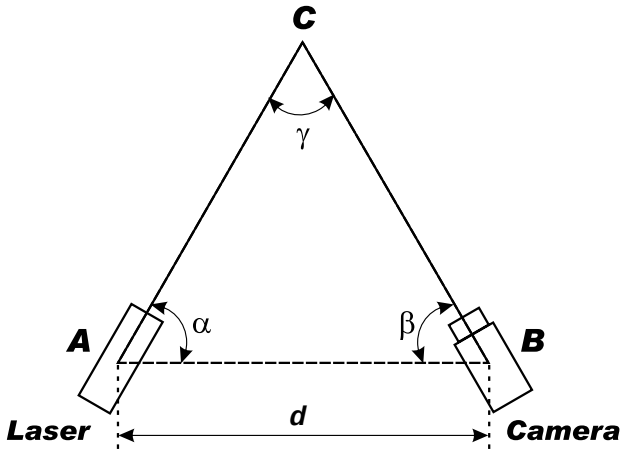

Fig. 1. (A) The triangulation principle.

Various mechanisms to replace image registration in range data integration have been proposed. These mechanisms use rail [9], rotating arm [10], mechanical arm [1], electromagnetic sensors [32], and optical sensors [39] to find the parameters of transformation functions that relate range coordinates determined during different scans to a global coordinate system. Natural [35], artificial [18], and light [19] markers have also been used to find the transformations.

Scanner heads containing one or two cameras and a laser source are not light and their use as hand-held devices becomes impractical when it is required to scan a large object over a long period of time. To simplify the scanning process, a mechanism that allows the user to hold and move only the laser projector to scan an object is proposed by Furukawa and Kawasaki [14]. Light-emitting diodes (LEDs) are attached to the laser, and from the images of the LEDs the equation of the laser plane creating each laser profile is determined during a scan.

In this paper a scanner mechanism is introduced that allows independent movement of the camera and the laser projector during a scan, enabling the user to hold a laser line generator the size of a pen while scanning an object, just like painting over the object with a paintbrush. One view of an object is obtained by fixing the camera and sweeping the laser over the object with hand. The camera is then moved to scan the object from a different view. A reference double-frame placed behind or in front of the object is used to automatically calibrate the scanner and relate the coordinate system of the camera to the coordinate system of the frame. Range data captured from different views of an object will be in the coordinate system of the frame independent of the camera position and thus will automatically come together without having to register them.

In the following sections, first, hand-held range scanners and range scanners that capture and automatically integrate multi-view range images are reviewed. Then, the hardware and software organizations of the proposed scanner are described. Next, the characteristics of the scanner are explored, and finally, example scans obtained by the scanner are presented.

2. Related work

To integrate range date captured from different views of an object, it is required to determine the relation between the coordinate system of the scanner and a global coordinate system as the scanner is moved. Image registration methods estimate such relations. Although image registration may be feasible when a small number of views is available, when tens or hundreds of views are involved, not only does error in computation of the transformations accumulate, but the process also becomes very time consuming.

Various mechanisms to determine the relation between the coordinate system of the scanner and a global coordinate system as the scanner is moved have been proposed. In a mechanism adopted by Cyberware [9], the laser projector and the camera are fixed in a scanner head and the head is moved with a constant speed along a vertical rail. Snapshots of laser profiles are obtained at uniform intervals and processed to obtain cross-sections of the object with uniformly spaced planes. By stacking the cross-sections, one side of the object is constructed. By using four synchronous heads and by processing the laser profiles from the four heads, complete cross-sections of the object with parallel and uniformly spaced planes are obtained. In this setup, since relations between the four cameras are fixed and known, data captured from the four views can be combined without registering them. This scanner is suitable for scanning the objects size of a human body. A smaller version of the scanner was constructed by Albamont and Goshtasby [2] for scanning objects the size of a person's head. A virtual laser rather than a real laser was used to scan very textured objects under very bright lights.

In a setup used by Curless and Levoy [8], the camera and the laser projector are both fixed but the object is translated at a constant speed and from uniformly spaced snapshots of the object, cross-sections of the object with uniformly spaced planes are determined and stacked to create a view of the object. Blais et al. [5] also keep the camera and the laser fixed but move the object by hand to reconstruct one view of the object. To merge range data captured from different object positions, a known pattern is projected to the object and the position of the pattern is determined via pattern matching. Starting from a coarse range image, progressively the range image is refined. Popescu et al. [33] project a pattern of 16 uniformly spaced laser points to the object under scan, and again through registration determine the relation between the new and existing range data and by merging newly captured range data with existing ones, gradually refine the model. Kofman and Knopf [22] collect several laser profiles at each scanner position and orientation in such a way that adjacent views have a sufficient overlap. Overlap between consecutive views is then used to register the acquired images and

progressively construct a model. Since parameters of adjacent views are not very different, an iterative closest-point (ICP) algorithm [4] is able to quickly determine the minor viewpoint difference between consecutive scans and progressively merge data from different views to create a model.

A rotating mechanism developed by Cyberware [10] rotates the scanner head about an axis at a fixed speed, obtaining uniformly spaced cross-sections of the object with vertical planes that have a uniform angular spacing and pass through the axis of rotation. Since the equation of the laser plane creating each laser profile is known, data generated by different camera positions can be related to a coordinate system that is positioned at the center of the scanner space, thereby automatically integrating data from different views. This scanner is suitable for scanning the head of a person or objects of similar sizes.

Mechanisms that allow the user to freely move the scanner head in 3-D while scanning an object have been developed by 3-D Scanners [1] and Kreon Technologies [23]. In these mechanisms, the scanner head is mounted on a mechanical arm, allowing accurate measurement of the position and orientation of the head during a scan. Range data computed for different laser profiles are transformed to a global coordinate system and merged to progressively reconstruct the object.

Attempts to determine the camera position and orientation using a global positioning system have been made also. Polhemus [32] has developed a range scanner that uses electromagnetic sensors to determine the position and orientation of the scanner at any time during a scan. Other range scanners using the global positioning idea to determine the pose of the scanner head during a scan are described by Fisher et al. [13], McCallum et al. [27], and Ferreira et al. [11].

Range data captured from different camera positions and orientations can be automatically combined if a number of points on the object can be seen by the camera at all times and the 3-D coordinates of the points can be determined. Hérbert [19] projects a number of fixed points to the object under scan and uses the images of the points to relate range data in the scanner coordinate system to a global coordinate system. Goshtasby et al. [18] attach a known physical marker to the object and by locating the marker in range images, transform range data captured from different views to the coordinate system of the marker, and integrate the images.

The position and orientation of the scanner head during a scan can be determined using a second sensor. Schulz [39] attaches multiple fixed and widely separated point lights to the scanner head and by locating the lights using a second sensor determines the absolute position and orientation of the scanner with respect to a global coordinate system. Individual light sources are distinguished by time-multiplexing their on–off states. A system developed by Northern Digital [31] attaches infrared reflectors to the scanner head and tracks the reflectors to determine the position and orientation of the head at any time by a stereo system.

Inclusion of one or two cameras and a laser source in a scanner head makes the head relatively heavy and unsuitable for lengthy scans. Attempts to separate the laser source and the camera(s) have been made. Furukawa and Kawasaki [14] and Takatsuka et al. [43] attach LEDs to the laser, and from the images of the LEDs determine the 3-D position and orientation of the laser during a scan. Instead of a laser projector, Bouguet and Perona [7] use the shadow of a rod cast onto an object for scanning. The position and orientation of the rod are determined using a reference plane that always contains a portion of the shadow of the rod during a scan. To eliminate the reference plane, Fisher et al. [12] use a rod with a triangular cross-section with each side of the rod painted differently so the faces can be identified in an image. Using the unique shape and geometry of the rod, the position and orientation of the rod with respect to the camera are determined from the image of the rod.

In this paper, a scanner mechanism is introduced that allows the camera and the laser projector to move independently. A double-frame is used to calibrate the camera as it is moved and also to determine the equation of the laser plane as it is swept over an object. Since all range values are measured in the coordinate system of the double-frame, captured range data from different views of an object will be in the same coordinate system and will automatically merge. The hardware and software of the scanner are described below.

3. Organization of the scanner

3.1. Hardware organization

The hardware organization of the scanner is depicted in Fig. 2. Fig. 2A shows the structure of the reference double-frame. W and H are, respectively, the width and height of the front frame; w and h are the width and height of the back frame; and d_x, d_y, d_z are distances between the lower-left corners of the front and back frames along the x, y, and z axes, respectively. Fig. 2B shows the relation between the camera, the laser plane, and the double-frame. Scanning is done by sweeping the laser light over an object by hand, just like painting over the object with a paintbrush. In this manner, dense range data can be captured in some areas while sparse data are captured in other areas. If desired, the laser sweeping process can be automated using a rotating mirror, a rotating arm, or a translation stage.

The world coordinate system is attached to the double-frame, and as long as the position of the object remains fixed with respect to the double-frame, object coordinates determined from different views will all be in the same coordinate system and thus will automatically merge to produce a single data set representing the object. The scanner, therefore, makes it possible to combine different-view range images of an object without registering them. Another characteristic of the scanner is that the camera and the

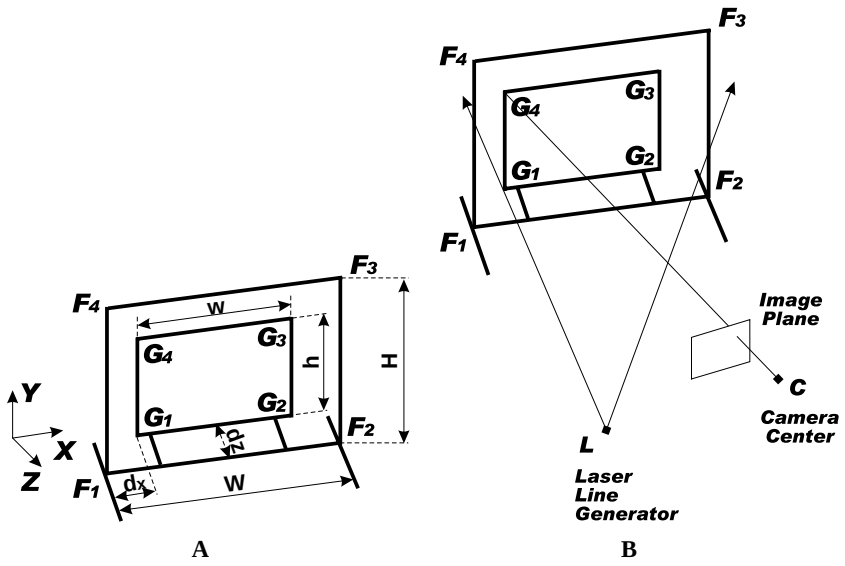

Fig. 2. (A) The structure of the reference double-frame. (B) Relation between the camera, the laser, and the double-frame.

laser source need not be fixed with respect to each other, and the user can move the laser independent of the camera to scan an object. Movement of the camera requires calibration of the scanner, which is achieved automatically. The calibration process is simple and is carried out once at the beginning of a new view. If the camera is continuously moved during a scan, the calibration is repeated with each image frame. The information to calibrate the scanner is present in each image frame. The uniqueness of the scanner is in the use of the double-frame. The double-frame not only makes it possible to integrate range images captured from different views, it provides a means to continuously calibrate the scanner as it is moved. There is often a need to move the camera and the laser independently to scan inside concavities and hard-to-see places.

The sizes of the objects to be scanned should be taken into consideration when designing the double-frame. The double-frame shown in Fig. 3, which was used for scanning human faces and objects of similar sizes, has the following dimensions: $W = H = 20.38$ in., $w = h = 16.25$ in., $d_x = 2.07$ in., $d_y = 0.12$ in., and $d_z = 6.62$ in. The distance between front and back frames determines the calibration accuracy in the Z direction. Small markers on the four corners of the front and back frames in Fig. 3 are used to locate the frames in the images. The markers must be continuously traced if the camera is moved. If the camera is fixed, the markers need to be located once at the beginning of a scan to calibrate the scanner.

Fig. 3. The actual double-frame during a scan.

In our setup, the front and back frames are fixed with respect to each other. The double-frame, however, can be made modular with removable parts for easy packing and assembly. The markers on each frame should be visible to the camera at all times. For obtaining scans from the front and back of an object, the markers should be placed at both sides of the frames. Since the dimensions of the frames are known ahead of time, the relation between the markers on the two sides of a frame can be determined. Therefore, independent of the viewpoint of the camera, range data can be captured with respect to the coordinate system of the double-frame.

The width of the laser line generator and the dimensions of the frames should be selected taking into consideration the sizes of the objects being scanned. When there is a need to scan very small objects, proportionately small frames and thin laser lines should be used. If a wider than necessary laser line is used, positional accuracy of laser stripes will be sacrificed. On the other hand, if a thinner than necessary laser line is used, the camera may not be able to detect the laser. The width of the laser line should be such that when it is cast on an object, it produces a laser stripe of thickness from one to several pixels. Some laser line generators allow adjustment of the thickness of the generated lines.

Although many laser range scanners use black-and-white cameras to capture and analyze images of the laser stripes, the scanner described here uses a color camera. Color acquisition offers some advantages over black-and-white cameras. First, knowing the spectral frequency of the laser, it is possible to enhance the laser stripes in images

for easier detection. Second, an object's real texture can be captured and mapped to the reconstructed geometry to create a realistic model of the object.

3.2. Software organization

As the laser light is swept over an object, the images captured by the camera are processed to obtain the 3-D coordinates of object points along the light stripes. In the following sections, details of the software modules that analyze the images and recover the 3-D geometry of the object under scan are provided.

3.2.1. Correcting the lens distortions

A camera's lens can distort the geometry of a captured image. Lens geometric distortions can be categorized into radial and tangential. Radial distortion occurs due to a lens' imperfect design and shifts image points radially toward or away from the lens center. Tangential distortion is caused by misalignment of the lens elements and shifts image points in the direction normal to the radii. Both distortions may be present in a camera, thus, displacing an image point from its true position in any direction.

Methods to correct images for lens distortions have been fully described elsewhere [16,21]. The process involves placing a known grid in front of the camera, obtaining an image of the grid, and using the coordinates of the ideal grid points and grid points in the image to determine a transformation function that will map the distorted grid to the ideal grid. Once the transformation is computed, it can be used to correct distortions in subsequently acquired images.

The scanner described in this paper uses a Panasonic camera model GP-US502 with a zoom lens. Fig. 4A shows a uniform grid and Fig. 4B shows an image of the grid obtained by our camera. The camera is focused at the grid such that its optical axis is normal to the grid and passes through the center of the grid shown by a "+" in the figure. When the camera is focused at the grid such that "+" is at the piercing point of the camera, a change in the zoom of the camera will not displace the "+" in the image. The distance of the camera to the grid is set approximately to the distance the camera is used to scan objects. From the coordinates of corresponding grid points a transformation function is found to resample the captured grid to the ideal grid. Fig. 4C shows result of this resampling, and Fig. 4D shows overlaying of the resampled grid and the ideal grid.

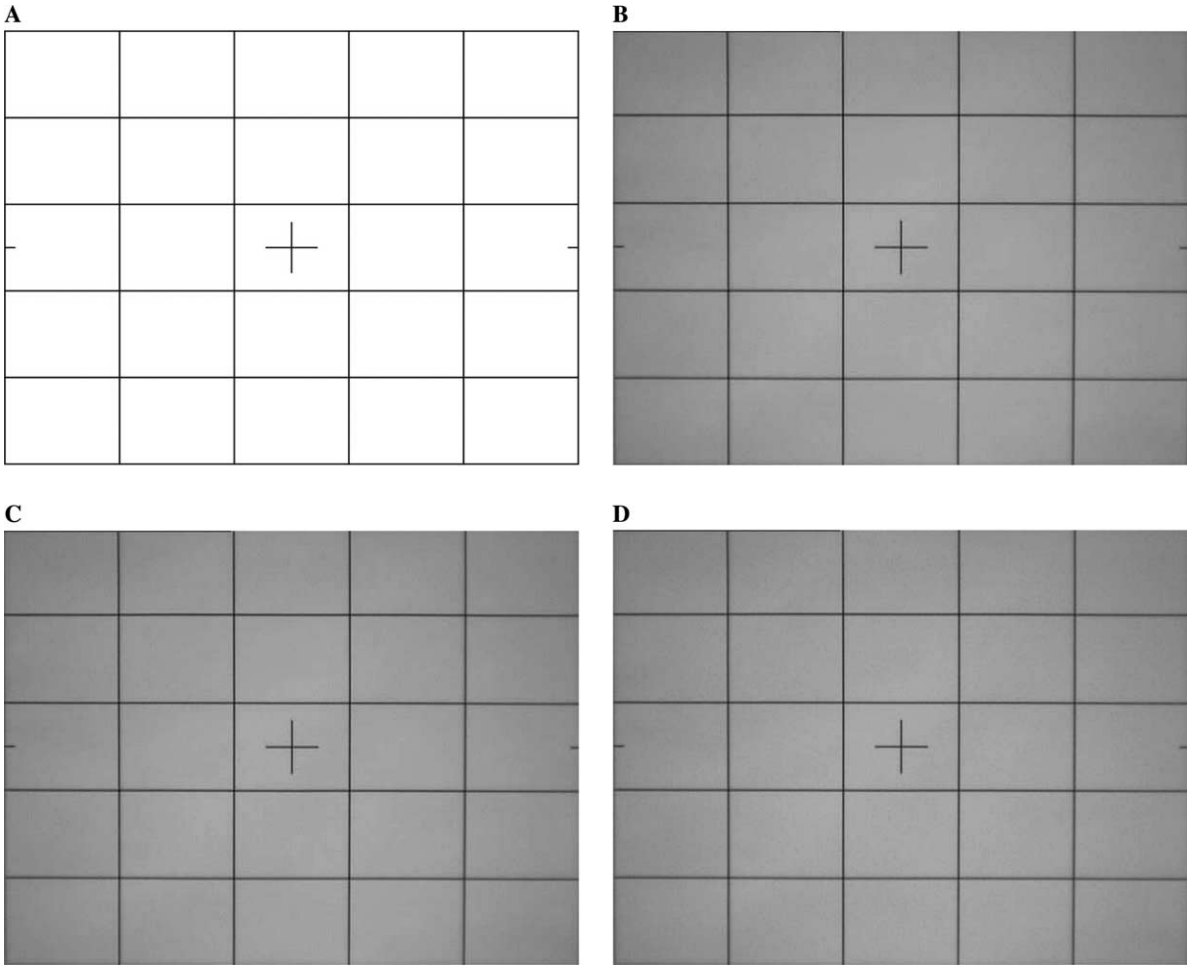

Fig. 4. (A) A uniform grid used to measure lens distortions. (B) An image of the grid obtained by our camera. (C) Resampling of (B) to align with (A) using coordinates of corresponding grid points in (A and B). (D) Overlaying of (A and C).

Displacement of image points by this camera was measured to be less than a pixel everywhere in the image space. In some cameras, lens distortions can displace image pixels by several pixels. We have been keeping the camera relatively far from the object and have been zoom in to obtain the images. The zooming process makes it possible to capture images with the object as well as the front and back frames appearing sharp.

3.2.2. Relation between image and reference frame coordinates

The relation between points in the front frame and their images can be written by a projective transformation:

$$X_f = \frac{a_1x + a_2y + a_3}{a_4x + a_5y + 1}, \tag{1}$$

$$Y_f = \frac{a_6x + a_7y + a_8}{a_4x + a_5y + 1}. \tag{2}$$

(X_f, Y_f) are coordinates of points in the front frame, (x, y) are coordinates of corresponding points in the image plane, and a_1–a_8 are the parameters of the transformation. The XY-plane is taken to be the plane of the front frame and the origin is taken to be the lower-left corner of the front frame. Knowing the coordinates of the four corners of the front frame and their images, parameters a_1–a_8 can be determined by solving a system of linear equations.

Similarly, the relation between points in the back frame and their images can be written as:

$$X_b = \frac{b_1x + b_2y + b_3}{b_4x + b_5y + 1}, \tag{3}$$

$$Y_b = \frac{b_6x + b_7y + b_8}{b_4x + b_5y + 1}. \tag{4}$$

Parameters b_1–b_8 of the transformation are again determined by knowing the coordinates of the corners of the back frame and the coordinates of their images. Every time the position, orientation, focal length, or zoom level of the camera is changed during a scan, the scanner is automatically calibrated. As the markers at the four corners of each frame are tracked in the images, the relation between frame points and image points is determined.

3.2.3. Equation of the laser plane

During a normal scan, the plane of laser intersects two borders of each frame as shown in Fig. 5. Assuming the intersections of the laser plane with the back frame are L_1 and L_2, and with the front frame are L_3 and L_4 (see Fig. 5), by determining the images of these four intersections, their 3-D coordinates can be determined from Eqs. (1)–(4) by the least-squares method.

Writing the equation of the laser plane by

$$Z = AX + BY + C, \tag{5}$$

parameters A, B, and C can be determined using the coordinates of the intersections of the laser plane with the front and back frames by least-squares. To determine the intersection of the laser plane with the left or right border in a frame, the laser point on the frame border that has the same X coordinate as that for the top or bottom marker is used, and to determine the intersection of the laser sheet with the top or bottom border in a frame, the laser point having the same Y coordinate as that for the left or right marker is used.

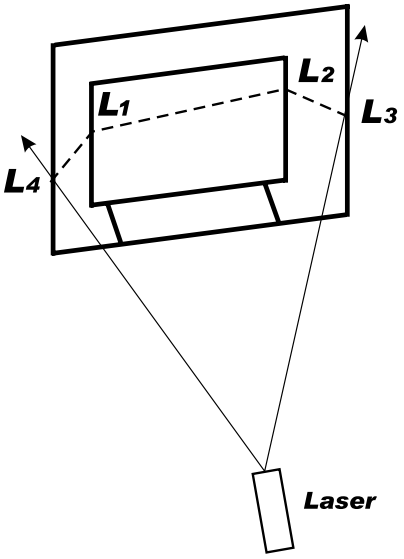

Fig. 5. Intersection of the laser plane with the frames.

If the plane of laser intersects the front or the back frame at only one point due to the occlusion by the object, rather than using the least-squares method, the parameters of the plane are obtained by solving the obtained system of three linear equations. If the laser plane intersects the frames at fewer than three points, the equation of the laser plane cannot be determined and so range data for the acquired laser profile cannot be computed. Sometimes by changing the direction of the laser more intersections with the frame borders can be created. For instance, if the right frame borders are occluded by the object and are not visible to the camera, and if the top and bottom frame borders are visible to the camera, the direction of the laser can be changed so the plane of laser would intersect the top and bottom frame borders and produce sufficient intersections to determine the equation of the laser plane.

3.2.4. Coordinates of the camera lens center

From the preceding discussions, it can be concluded that each point in the image plane corresponds to a point in the front frame and a point in the back frame. The three points lie on a ray that passes through the lens center. Fig. 6 shows this geometry. Let us suppose the line connecting the lens center to the lower-left corner of the back frame (point G_1) intersects the front frame at f_1. The coordinates of point C (the lens center) are not known, but the coordinates of G_1 in 3-D are known, and the coordinates of f_1 can be determined from the discussion in Section 3.2.2. Similarly, the rays that connect points G_2, G_3, and G_4 to their

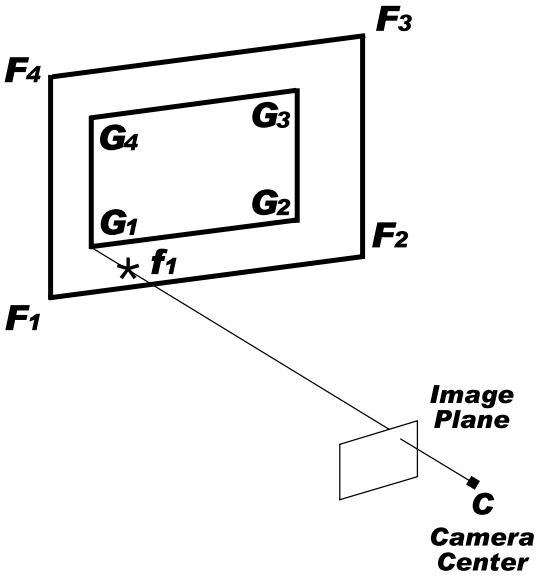

Fig. 6. Relation between the camera lens center and the front and back frames.

images can be determined. All these rays should pass through the lens center. Theoretically, from the intersection of any two such rays it should be possible to determine the position of the lens center. But because of the discrete nature of pixel positions, the lines may not intersect at lens center. They will, however, pass close to each other near the lens center.

The position of the lens center is estimated to be the point in 3-D whose sum of squared distances to the four rays is minimum. Assuming the 3-D coordinates of points G_1 and f_1 are (X_1, Y_1, Z_1) and (X'_1, Y'_1, Z'_1), respectively, the parametric line passing through them can be written as:

$$X = X_1 + (X'_1 - X_1)t, \tag{6}$$

$$Y = Y_1 + (Y'_1 - Y_1)t, \tag{7}$$

$$Z = Z_1 + (Z'_1 - Z_1)t. \tag{8}$$

Assuming the coordinates of the lens center are (X_c, Y_c, Z_c), the square distance of the lens center to the point with parameter t on the line is

$$d^2 = [X_1 + (X'_1 - X_1)t - X_c]^2 + [Y_1 + (Y'_1 - Y_1)t - Y_c]^2 + [Z_1 + (Z'_1 - Z_1)t - Z_c]^2, \tag{9}$$

the value of t that minimizes d^2 can be determined by finding the derivative of d^2 with respect to t, setting it to zero, and solving the obtained equation. Denoting the parameter obtained in this manner by t_1, we find

$$t_1 = \frac{-(X_1 - X_c)(X'_1 - X_1) - (Y_1 - Y_c)(Y'_1 - Y_1) - (Z_1 - Z_c)(Z'_1 - Z_1)}{(X'_1 - X_1)^2 + (Y'_1 - Y_1)^2 + (Z'_1 - Z_1)^2}. \tag{10}$$

Similarly, rays connecting G_2, G_3, and G_4 to their images can be determined and the point on each ray closest to (X_c, Y_c, Z_c) can be computed. Assuming points on the three rays closest to the lens center have parameter coordinates t_2, t_3, and t_4, using Eq. (9), the sum of squared distances of point (X_c, Y_c, Z_c) to the four rays can be written as

$$E_2 = \sum_{i=1}^{4} [X_i + (X'_i - X_i)t_i - X_c]^2 + [Y_i + (Y'_i - Y_i)t_i - Y_c]^2 + [Z_i + (Z'_i - Z_i)t_i - Z_c]^2. \tag{11}$$

Substituting t_1, t_2, t_3, and t_4 into Eq. (11), E_2 will be in terms of X_c, Y_c, and Z_c. To determine the X_c, Y_c, and Z_c that minimize E_2, partial derivatives of E_2 with respect to X_c, Y_c, and Z_c are determined and set to zero and the obtained system of linear equations is solved for X_c, Y_c, and Z_c.

3.2.5. Coordinates of object points

Suppose the image of an object point **P** is point **q** in the image plane as shown in Fig. 7. Point **q** also corresponds to a point in the back frame. Let us call that point **Q**. The coordinates of **Q** can be determined from the coordinates of **q** according to the discussion in Section 3.2.2. The equation of the laser plane can also be determined from the coordinates of the intersections of the laser plane with the front and back frames according to the discussion in Section 3.2.3. Knowing the coordinates of the lens center **C** and the coordinates of point **Q**, the intersection of the ray passing through **C** and **Q** with the laser plane finds the object point **P**.

3.2.6. Data integration and estimation of missing data

Range data captured from an object may contain holes at places where object color is very dark or the object is occluded from the camera. To fill in the holes, a local weighted averaging scheme is adopted. To estimate the

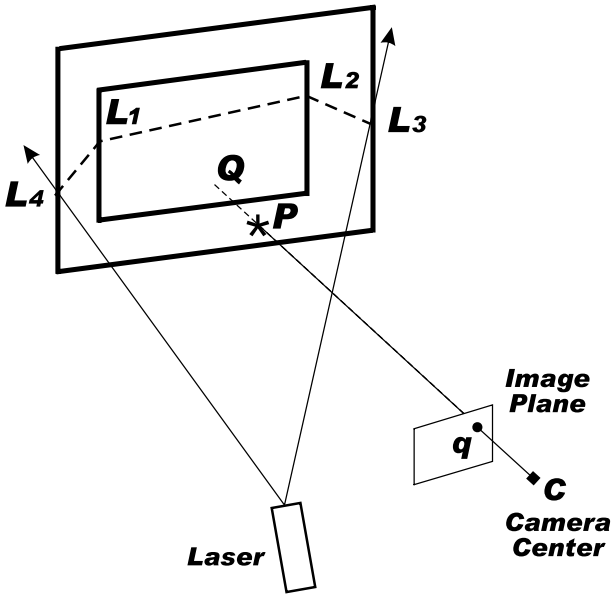

Fig. 7. Finding the coordinates of an object point **P** in 3-D from the coordinates of its image point **q**.

(X, Y, Z) coordinates of the object point corresponding to pixel (x, y), 3-D coordinates of object points corresponding to pixels surrounding (x, y) are used in the following weighted averaging method:

$$X = \sum_{i=1}^{n} W_i(x,y)X_i, \tag{12}$$

$$Y = \sum_{i=1}^{n} W_i(x,y)Y_i, \tag{13}$$

$$Z = \sum_{i=1}^{n} W_i(x,y)Z_i, \tag{14}$$

where n is a small number such as 8 and (X_i, Y_i, Z_i) are the coordinates of the object point corresponding to the ith pixel closest to (x, y). $W_i(x, y)$ is a monotonically decreasing weight function whose value at (x, y) is proportional to the inverse distance of (x, y) to (x_i, y_i), normalized such that $\sum_{i=1}^{n} W_i(x,y) = 1$. Letting

$$w_i(x,y) = \{(x-x_i)^2 + (y-y_i)^2 + \delta\}^{-\frac{1}{2}}, \tag{15}$$

we will have

$$W_i(x,y) = \frac{w_i(x,y)}{\sum_{i=1}^{n} w_i(x,y)}. \tag{16}$$

(x, y) is the pixel with the missing range data, and (x_i, y_i) is the ith pixel closest to (x, y) where its range data are known. δ controls the localness of the estimation. The smaller the δ the more will be the effect of the pixel closest to (x, y) on the estimated value, while the larger the δ the more equal will be the influence of all n pixels on the estimated value.

Formulas (12)–(14) are used when carrying out hole-filling on a single side of an object. When data from multiple sides of an object are captured and integrated, a set of points with coordinates (X, Y, Z) will be obtained. To organize the points, they are cylindrically parametrized. Parameters (u, v) are assigned to point (X, Y, Z) in such a way that v will be proportional to Z, and u will be proportional to the angle vector (X, Y) in the XY-plane makes with the X-axis, and u and v both vary from 0 and 1. Irregularly spaced range data obtained by integrating different views are resampled to a regular grid starting from $u = 0$ and $v = 0$ up to $u = 1$ and $v = 1$ with increments selected to produce the desired grid size for rendering. In formulas (12)–(14), when the points are cylindrically parametrized, (x, y) is replaced with (u, v) and (x_i, y_i) is replaced with (u_i, v_i). This sampling will produce a regular rectangular grid, which can be rendered for viewing purposes. The process not only

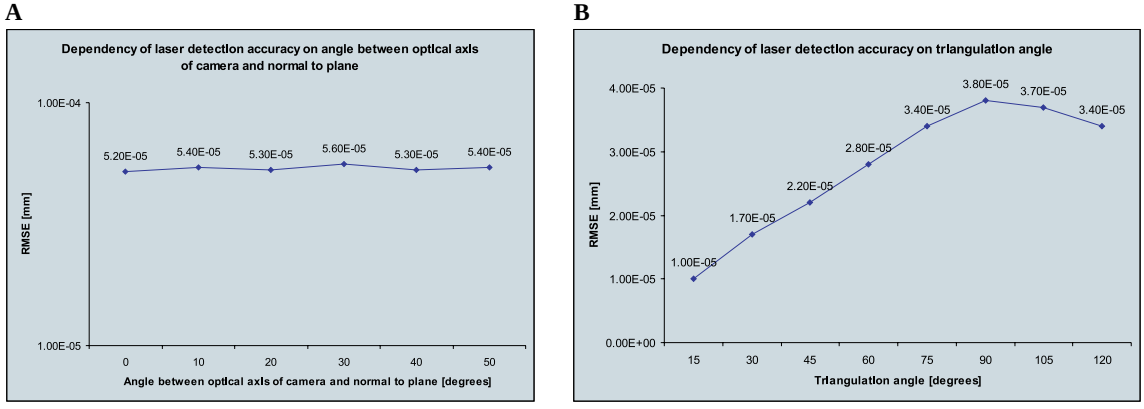

Fig. 8. Dependency of laser positional accuracy on (A) surface orientation and (B) triangulation angle.

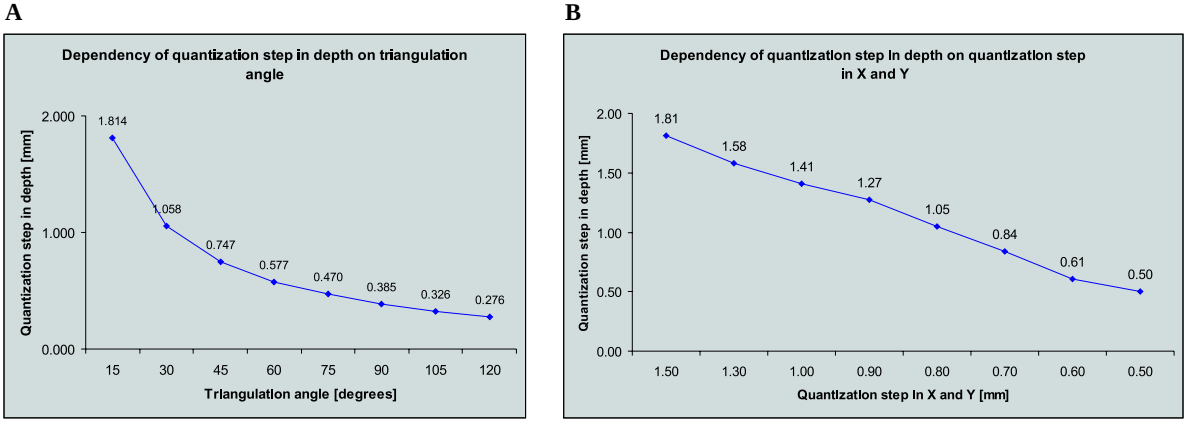

Fig. 9. Dependency of quantization in depth on (A) triangulation angle and (B) quantization step in X and Y.

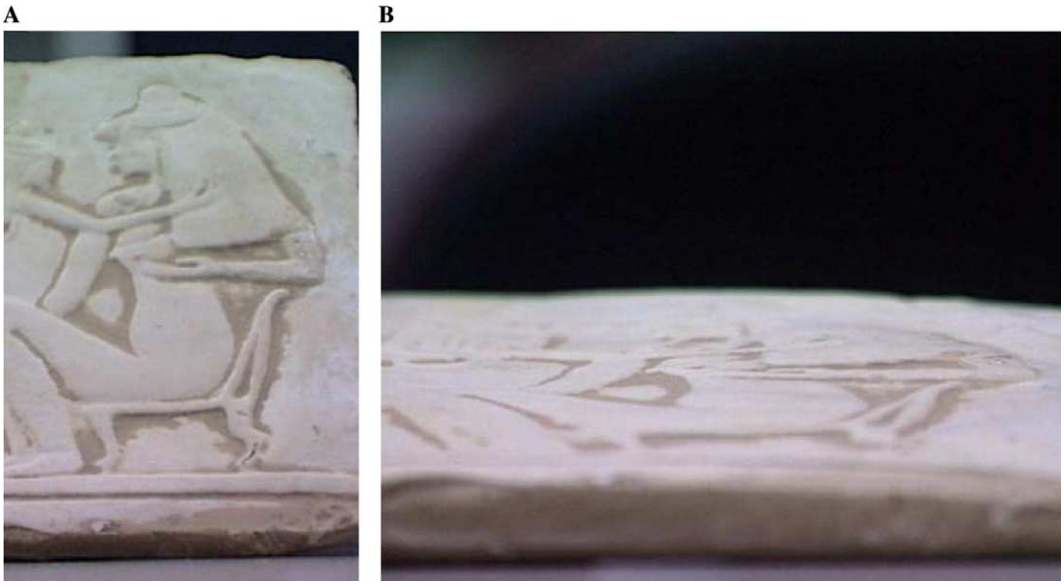

Fig. 10. (A) An Egyptian art piece. (B) A side view of the art piece showing its relief.

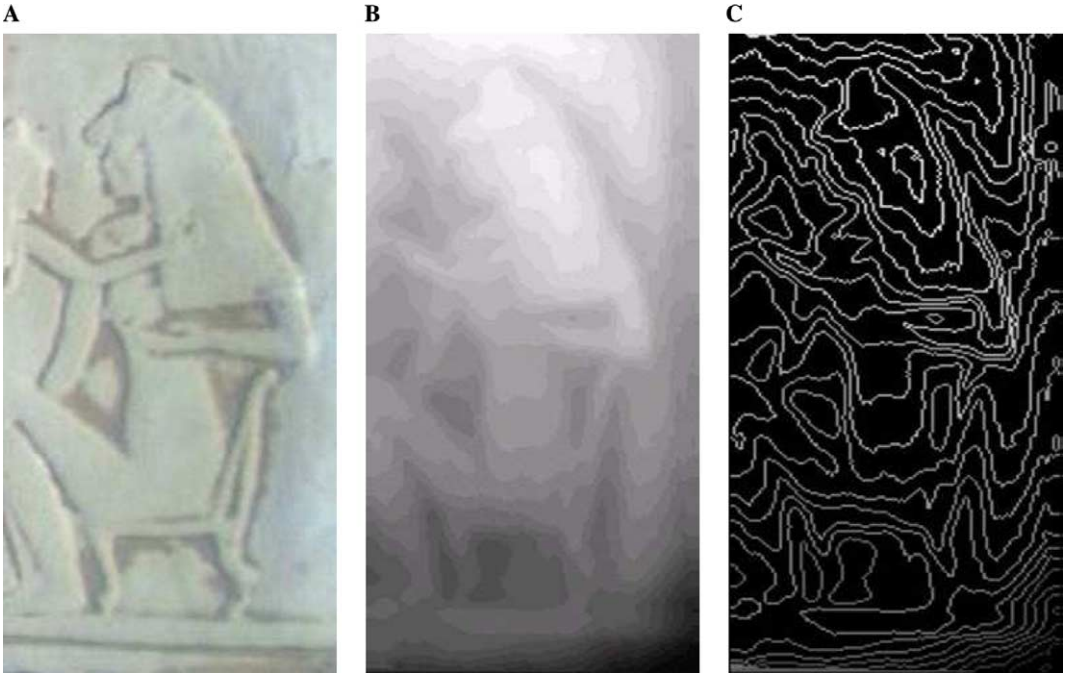

Fig. 11. (A) An image of the scanned plaque known as "Egyptian Dancers." (B) Depth map of the plaque. (C) Isovalued depth contours of the plaque with 0.43 mm spacing.

fills in missing data, it eliminates duplicate points, thins dense range data obtained in overlapping areas, and smoothes noise. In our implementation, the created grid is considered the control mesh of a uniform B-spline surface and the B-spline surface is used to render the constructed model. A B-spline surface enables viewing of the reconstructed object from up close with smooth shading. If the object does not close from one side, points on the boundary of the object are repeated to maintain a regular grid in the uv space. This facilitates rendering of the reconstructed object by varying u and v from 0 to 1 at all times.

The above parametrization is suitable for genus-zero objects. For complex objects with holes and handles a more elaborate integration and hole-filling method is needed. Various algorithms for this purpose have been developed. The methods can be categorized into surface fitting, mesh integration, and implicit surface approaches. In the surface fitting method, a surface is fitted to range points and the surface is used to represent the scanned

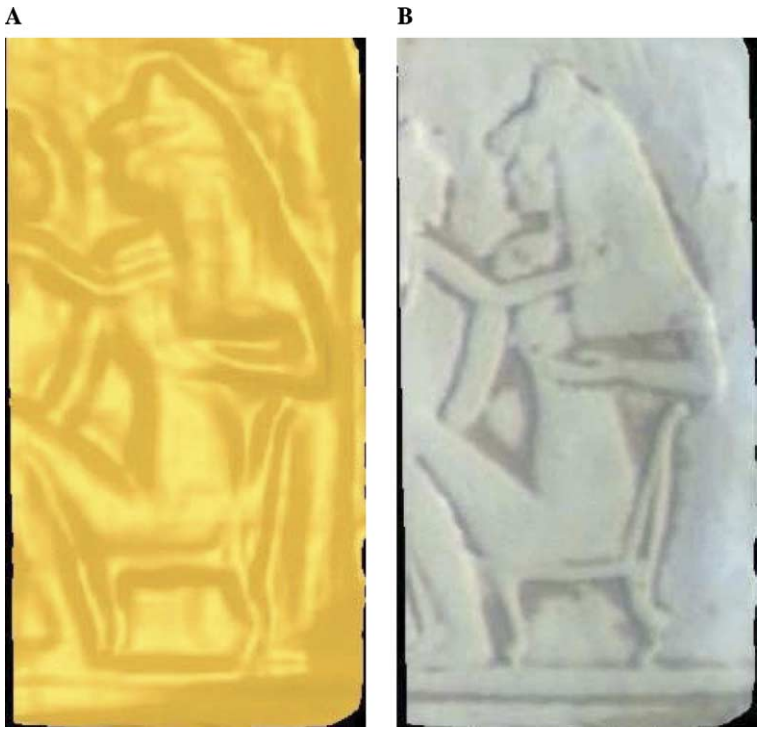

Fig. 12. (A) B-spline surface approximation of the range data. (B) Texture-mapped surface showing the reconstructed plaque.

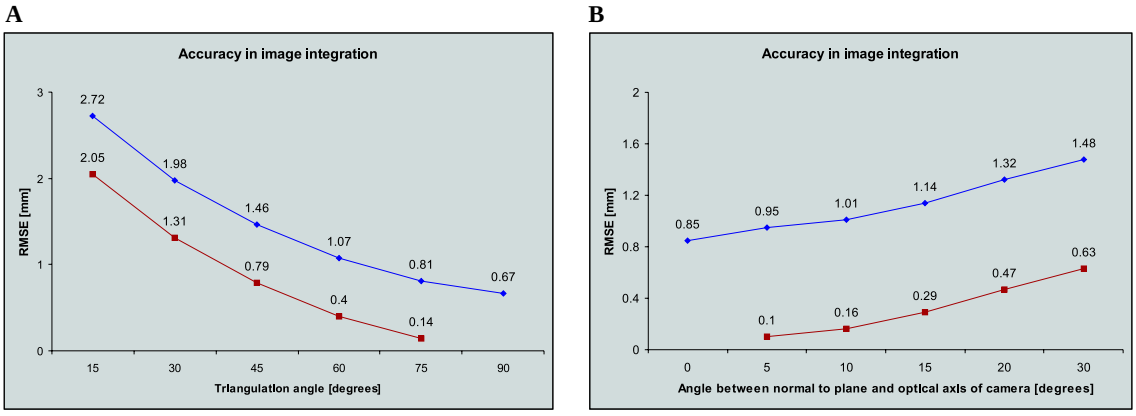

Fig. 13. Dependency of data integration accuracy on (A) the triangulation angle and (B) the angle between camera orientation and surface normal.

object [17,24,37,42]. The method described above falls into this category. In the mesh integration method, range data from different views are triangulated and the meshes are merged. Boissonnat [6] uses a graph-based approach to determine correspondence between overlapping meshes and retriangulates the overlapping meshes to merge the meshes. Soucy and Laurendeau [40] use canonic subsets of the Venn diagram representing the overlap area between two meshes to merge the meshes. In the implicit surface approach, each data point is considered a field that is zero at the center and monotonically increases in strength with distance to the center point. The sum of the fields is computed and locally minimum field values are traced to obtain the surface. Instead of locally minimum field values, isovalued field values may be traced if signed distances are used in place of monotonically increasing fields. If the volume containing a triangular mesh is quantized such that voxels on one side of a triangle are given positive values while voxels on the other side are given negative values with magnitudes proportional to their distances to the plane of the triangle, and if such signed distances are added for all triangles, zero-valued voxels will produce the bounding surface of the object. This approach has been taken by Curless and Levoy [8], Sagawa and Ikeuchi [36], and Hilton et al. [20]. Masuda [26] and Tubic et al. [45] use signed distances to register as well as to integrate range data.

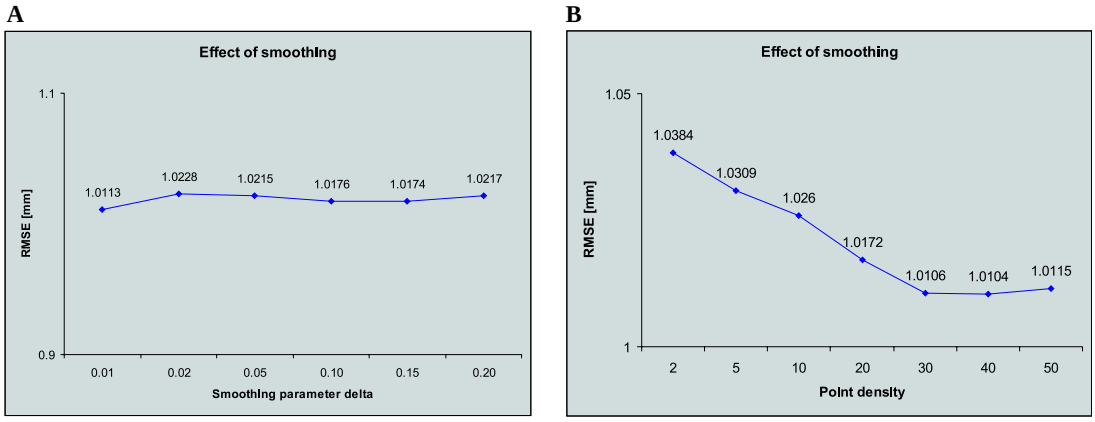

Fig. 14. Dependency of the hole-filling process on (A) parameter δ and (B) parameter n of formulas (12)–(16).

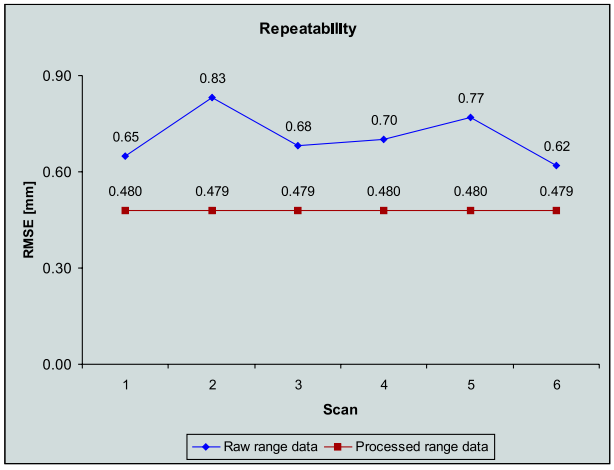

Fig. 15. Scanner repeatability.

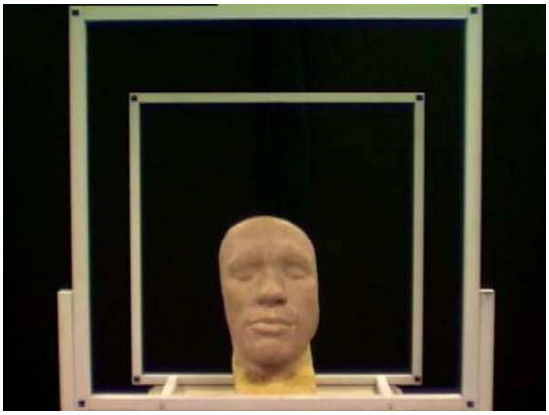

Fig. 16. Model of a human face used in an experiment.

3.2.7. Texture mapping

It is often necessary to map the natural texture of an object to the reconstructed object to give it a natural look. For texture mapping, the correspondence between object coordinates and texture coordinates should be determined. A reconstructed surface is quantized with uniform spacing by varying u and v from 0 to 1 with small increments. This quantization produces a regular grid of points. Four adjacent points form a quadrilateral, whose texture is obtained from a rectangular area in the image. The increment in u and v determines the number of quadrilaterals obtained and controls the quality of the generated surface. The smaller the increment, the more detailed the reconstructed surface will be. Too small an increment, however, will only increase the computation time without improving the rendering quality. For instance, when the four corners of a quadrilateral map to an image area smaller than 2×2 pixels, no added accuracy will be achieved by taking smaller increments.

The above simple procedure works when mapping the texture from a single view of an object to the reconstructed surface. In many situations it is required to combine texture from multiple views of an object to reconstruct the object in its entirety. Texture mapping in multiple views is achieved by first determining the texture coordinates for each recovered object point in 3-D. In this way, at each point on the reconstructed surface there will be not only the (X, Y, Z) coordinates of the point, but there also will be the (R, G, B) color values of the point. Therefore, instead of fitting a surface with three components to the obtained range data as described in Section 3.2.6, a surface with six components is fitted to the range and texture data. By varying u and v from 0 to 1, the surface is generated using the first three components of the surface and its texture is generated using the last three components of the surface. This process will not only fill in missing range values, it will also fill in the missing texture values and average the range and color values in overlap areas.

3.2.8. Scanner calibration

Calibration is the process of determining the relation between points in an image and points in 3-D. The calibration process, in effect, determines the parameters of this relation so that, given an image point, the coordinates of the point in 3-D can be determined.

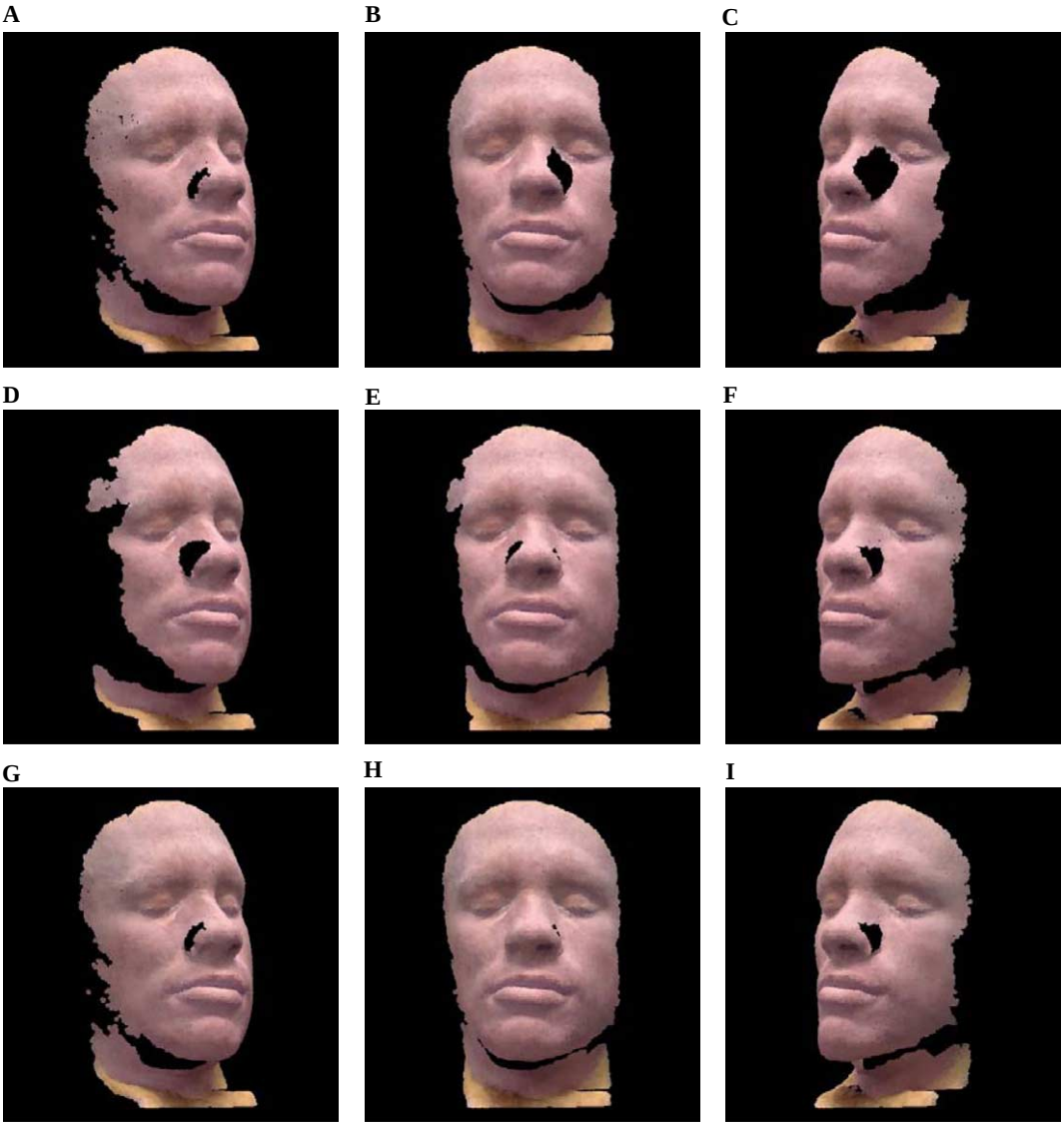

Fig. 17. (A–C) Three views of a range data set captured by sweeping the laser from the left side. (D–F) Three views of a range data obtained by sweeping the laser from the right side. Both scans were obtained at the same camera position. (G–I) Integration of the two range data sets.

To establish correspondence between image points and points in the front and back frames, according to the discussion in Section 3.2.2, it is required to determine the coordinates of the markers on the frames in an acquired image. The coordinates of the markers on the frames in 3-D are known. In the current setup, the markers are blue rectangular spots at the four corners of each frame. The markers may be made of light-emitting diodes with distinct colors for the front and black frames to make them more easily distinguishable in the images.

As explained in Section 3.2.3, the position and orientation of the laser plane is determined in each image after the relation between image points and points in the front and back frames are determined. Also, the position and orientation of the camera is determined from the coordinates of the markers on the four corners of the frames as outlined in Section 3.2.4. Once the camera position and orientation, and the equation of the laser plane is determined, the coordinates of points in the scene can be determined from their images using the procedure outlined in Section 3.2.5.

There are a few sources of error that could degrade the calibration process. For instance, due to the digital nature of images and the presence of noise, the center of a marker could be off by a pixel or two. The intersection of a laser plane with the frame border could be displaced by a pixel due to the digital nature of images. Determination of camera position depends on the intersections of laser lines with the frame borders; therefore, errors in determining the intersections will carry over to errors in camera position, and errors in camera position directly affect accuracy in computed depth values. The errors and ambiguities can be reduced or removed by using very small LED markers, a brighter laser, a darker environment lighting, and a higher resolution camera.

Fig. 18. (A–C) Range data captured from two camera views after hole-filling in image space. (D–F) B-spline surface approximation of the combined range data, representing hole-filling in 3-D. (G–I) Reconstructed model face in texture-mapped form.

4. Characteristics of the scanner

To determine the accuracy of the scanner and to investigate its characteristics, a number of experiments were carried out. A single plane was used in the experiments. Low curvature object points that can be locally considered planes are expected to have the errors reported here. Errors at high curvature points on an object may be higher than those reported here.

4.1. Laser positional accuracy

To trace the spine of a laser profile, a peak detector is applied to the red component of each image frame. The red component of an image is used because the laser used in the scanner has a reddish color. Each digital peak is replaced with the peak of a biquadratic surface fitting the 3×3 window centered at the digital peak. Since the peak of a biquadratic surface can be determined with subpixel accuracy, the process will in effect trace the spine of a laser profile with subpixel positional accuracy. A review of various methods for tracing the spine of a laser profile has been provided by Naidu and Fisher [29].

To evaluate the positional accuracy of laser profiles and to determine the characteristics of the scanner under different scanning conditions, two experiments were carried out. In the first experiment a plane was placed inside the double-frame and scanned while rotating it about a horizontal axis and keeping the triangulation angle at about 90°. As the plane rotates, the width of the laser profile changes. The accuracy of the laser points determined at each orientation of the plane is determined by first finding the equation of the laser plane from the intersection of the laser with the four frame borders. Then, the root-mean-squared (RMS) distance of the laser points in 3-D to the plane is determined and depicted in Fig. 8A. As can be observed,

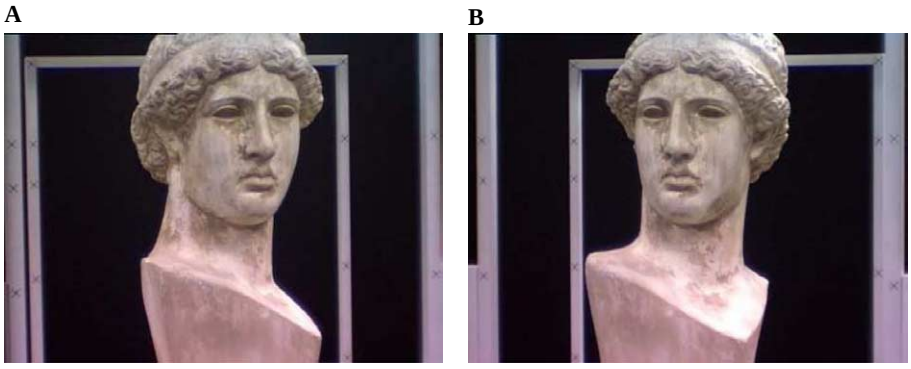

Fig. 19. A Greek statue (A) from left view and (B) from right view.

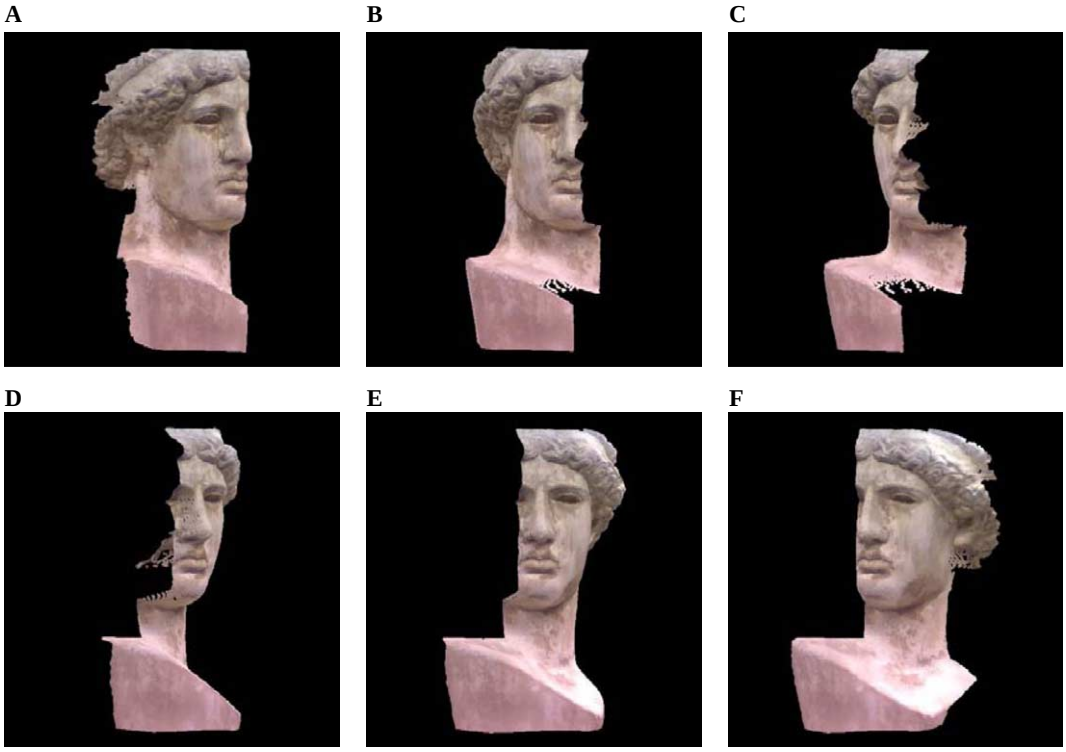

Fig. 20. (A–C) Range data obtained from the left camera view. (D–F) Range data obtained from the right camera view.

the errors are very small and hardly change with the change in surface orientation.

In the second experiment, the triangulation angle is changed while keeping the plane parallel to the XY-plane within the double-frame. The obtained RMS errors are depicted in Fig. 8B. As the triangulation angle is increased, the laser positional error increases up to about 90° and then it decreases. This behavior is puzzling and it is not clear why it happens. RMS error is very small over the entire usable range of triangulation angles though.

4.2. Depth resolution

Resolutions in X and Y directions are the reverse of quantization steps in X and Y directions, which are the dimensions of image pixels. If a pixel covers a 1 mm × 1 mm area on an object, the quantization step in X and Y directions will be 1 mm. To determine the quantization step in Z direction, a translation stage is used. Suppose a horizontal laser stripe on a vertical plane that is parallel to the XY-plane falls on scanline h_1 in an image. If after moving the plane by d mm parallel to itself the horizontal stripe shifts to scanline h_2, the quantization step in Z direction (in depth) will be $d/(h_2 - h_1)$ mm and the resolution will be $(h_2 - h_1)/d$ pixels per mm. To determine the dependency of quantization step in depth on the triangulation angle, an experiment was carried out for various triangulation angles and the obtained results are depicted in Fig. 9A. Depth resolution increases (quantization step in depth decreases) as the triangulation angle is increased. Depth resolution also depends on the zoom level. As larger areas are scanned by zooming out, resolution in depth

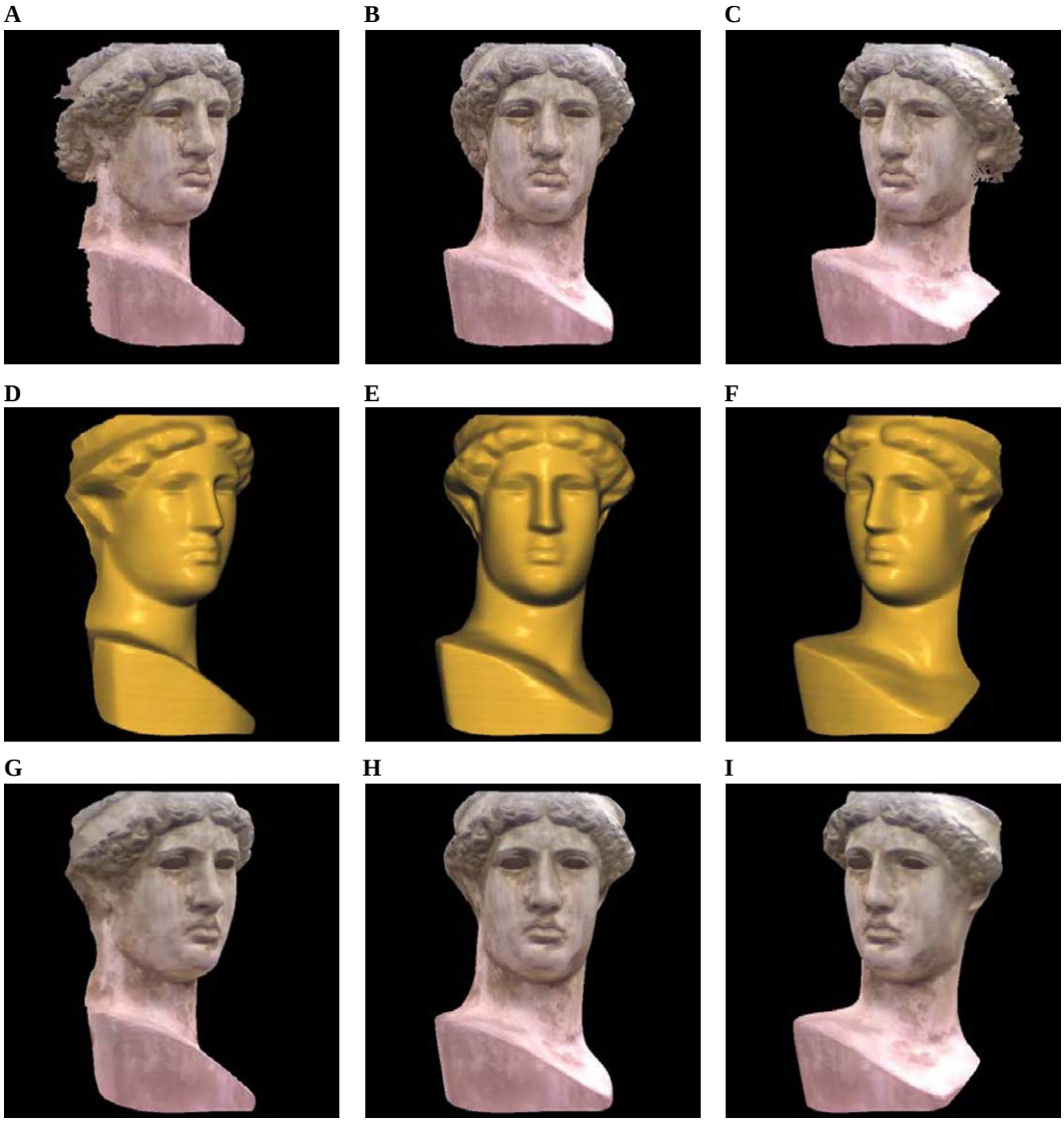

Fig. 21. (A–C) Integrated range data after hole-filling. (D–F) Geometric reconstruction of the statue by fitting a B-spline surface to the range data. (G–I) The reconstructed statue in texture-mapped form.

decreases as resolution in X and Y decreases, or similarly the quantization step in depth decreases as pixel size decreases. This is depicted in Fig. 9B.

To determine quantization in depth in an actual scan, an Egyptian art piece as shown in Fig. 10 was used. The width of the portion of the plaque visible in Fig. 10A is 312 pixels. These 312 pixels corresponded to 161 mm on the plaque. Therefore, the quantization step in X direction is 161/312 or about 0.52 mm. Since the aspect ratio of pixels in the images by our camera is 1, it can be concluded that quantization step in Y direction is also about 0.52 mm.

An image of the plaque from the side view is shown in Fig. 10B to demonstrate the amount of relief on the plaque. To determine the quantization step in depth, the actual difference between the highest point on the plaque and the lowest point on the plaque was found visually with a ruler to be about 3 mm. The plaque was then placed in the scanner parallel to the frames and scanned with a triangulation angle in the range of about 90°, and the depths of points on the plaque were determined. Disparity of seven pixels was obtained between the farthest and nearest points on the plaque. Therefore, the quantization step in depth is 3/7 or 0.43 mm. Further decrease of the quantization step in depth can be achieved by either zooming in and scanning a smaller area of the plaque or using a higher resolution camera. Captured depth values were mapped to 0–255 for enhanced viewing in Fig. 11B. Isovalued depth contours with 0.43 mm spacing in height are shown in Fig. 11C. A B-spline surface approximation of the range data is shown in Fig. 12A, and the texture-mapped surface is depicted in Fig. 12B. Details not visible in the plaque intensity image have become visible in the geometry image. The surface fitting process has smoothed digital noise in estimated depth values and has restored the smooth geometry of the plaque.

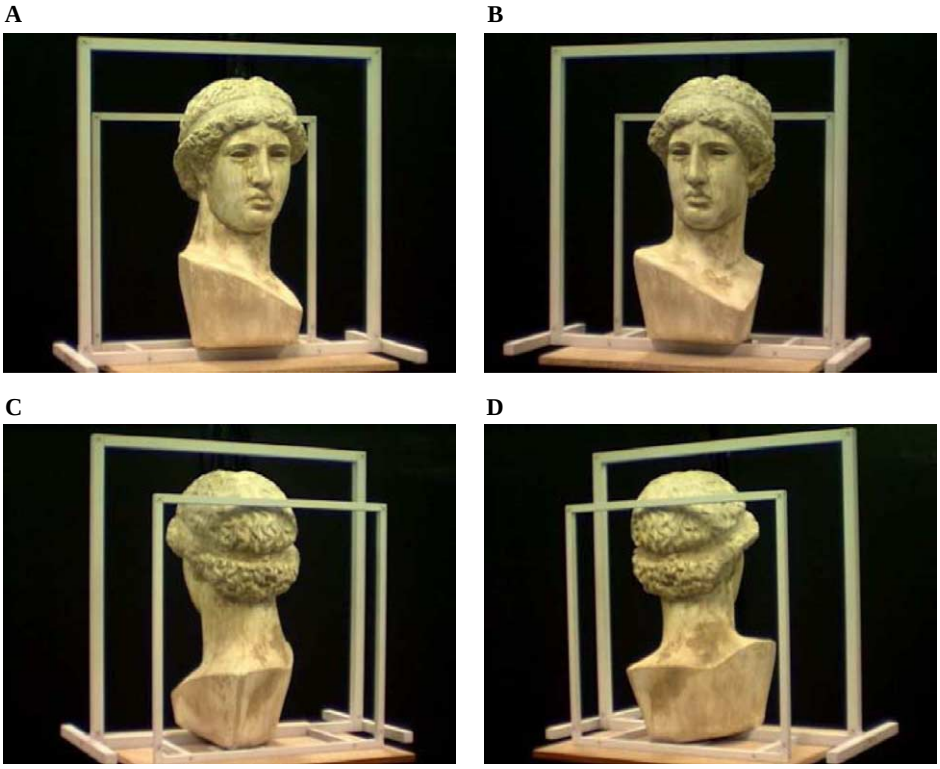

Fig. 22. Four views of a Greek statue. (A) Front-left view. (B) Front-right view. (C) Back-left view. (D) Back-right view.

4.3. Data integration characteristics

To determine the characteristics of the range data integration process outlined in Section 3.2.6, two experiments were carried out. In one experiment, a plane placed at $Z = 0$ was scanned several times under different triangulation angles. The camera was kept fixed but the laser orientation was changed to obtain the scans. Knowing the true position of the plane in 3-D, the RMS distance between the 3-D laser points and plane $Z = 0$ was determined in each case. The top plot in Fig. 13A shows the RMS distances in millimeter. The bottom plot shows the RMS error to be expected when integrating data at two different triangulation angles. For instance, RMS error of 0.79 mm in the bottom plot indicates the error to be expected when integrating overlapping range data scanned with triangulation angles 45° and 90°. The graph shows that if a range scan obtained with triangulation angle 45° is integrated with a range scan acquired with triangulation angle 60°, the RMS integration error is expected to be 0.39 mm.

In the second experiment, the orientation of the laser was kept fixed for all the scans, but the camera was moved with respect to the plane. Again, the RMS distance between computed 3-D laser points and the $Z = 0$ plane was determined for each scan and plotted in Fig. 13B. The plot at the top shows RMS error as a function of the angle between the optical axis of camera and the normal to the plane. The bottom plot shows the RMS error to be expected when two laser scans with different camera positions are merged. For instance, 0.16 mm will be the expected RMS error of integrating range data scanned once with the camera optical axis parallel to the Z-axis and another time having an angle of 10° with it.

4.4. Characteristics of the hole-filling process

Two parameters influence the hole-filling process of Section 3.2.6. They are δ in formula (15) and n in Eqs. (12)–(14). The hole-filling process not only fills in the holes but it smoothes the range data also. In an experiment, the range data captured for the plane at $Z = 0$ with triangulation angle about 90° was smoothed according to formulas (12)–(14) by varying δ from 0.01 to 0.2. Fig. 14A shows that RMS error in estimated range values increases only slightly with increase in δ. The cost of smoothing noise is the reduction in accuracy of estimated range values.

In another experiment, the number of points used in estimating missing range data or smoothing existing range data was varied from 2 to 50. As n is increased, RMS estimation/smoothing error decreases with increasing n up to 30, beyond which error starts to increase. This figure shows estimation/smoothing error when a plane is scanned. If a curved surface is scanned, a different error plot is expected. For curved surfaces, n greater than 10 is not recommended as the smoothing process will smooth critical surface details. Parameters n and δ are set to fixed values 10 and 0.1, respectively, in our scanner.

Fig. 23. (A–C) Range data obtained from the front camera views. (D–F) Range data obtained from the back camera views. (G–L) Reconstruction of the statue by integrating range data from the four views.

4.5. Repeatability

Since the laser line generator and the camera can move independently during a scan, to determine the repeatability of the scanner, the plane $Z = 0$ was scanned with about the same triangulation angle, about the same camera position and orientation, and about the same laser orientation a number of times and the RMS error of 3-D laser points to plane $Z = 0$ for each case was computed and plotted in Fig. 15. The top plot shows the RMS reconstruction error when raw range values (without hole-filling/smoothing) are used. Since the laser is swept with hand, the spacing be-

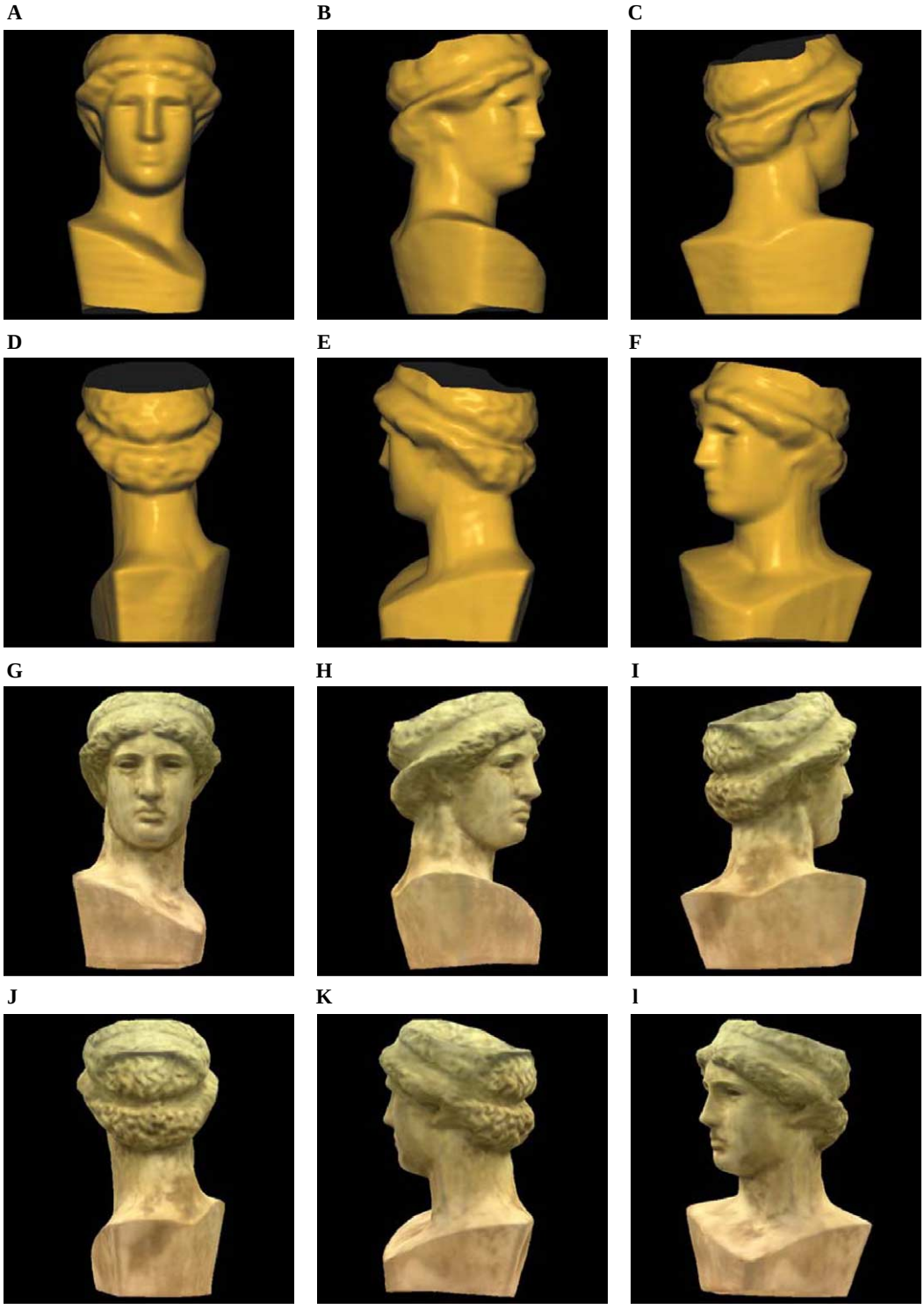

Fig. 24. (A–F) B-spline surface approximation of the combined range data set. (G–L) Texture-mapped surface representing the reconstructed statue.

tween the laser profiles is not uniform and the density of captured range points vary from scan to scan. Therefore, RMS errors slightly vary from scan to scan. However, when the hole-filling/smoothing step is applied to the captured data, the scanning process becomes very stable, producing almost the same result.

5. Example scans

In this section, example scans produced by the scanner are presented. In the first example, a model face was scanned from two separate laser positions but with the same camera position. When the position of the laser is

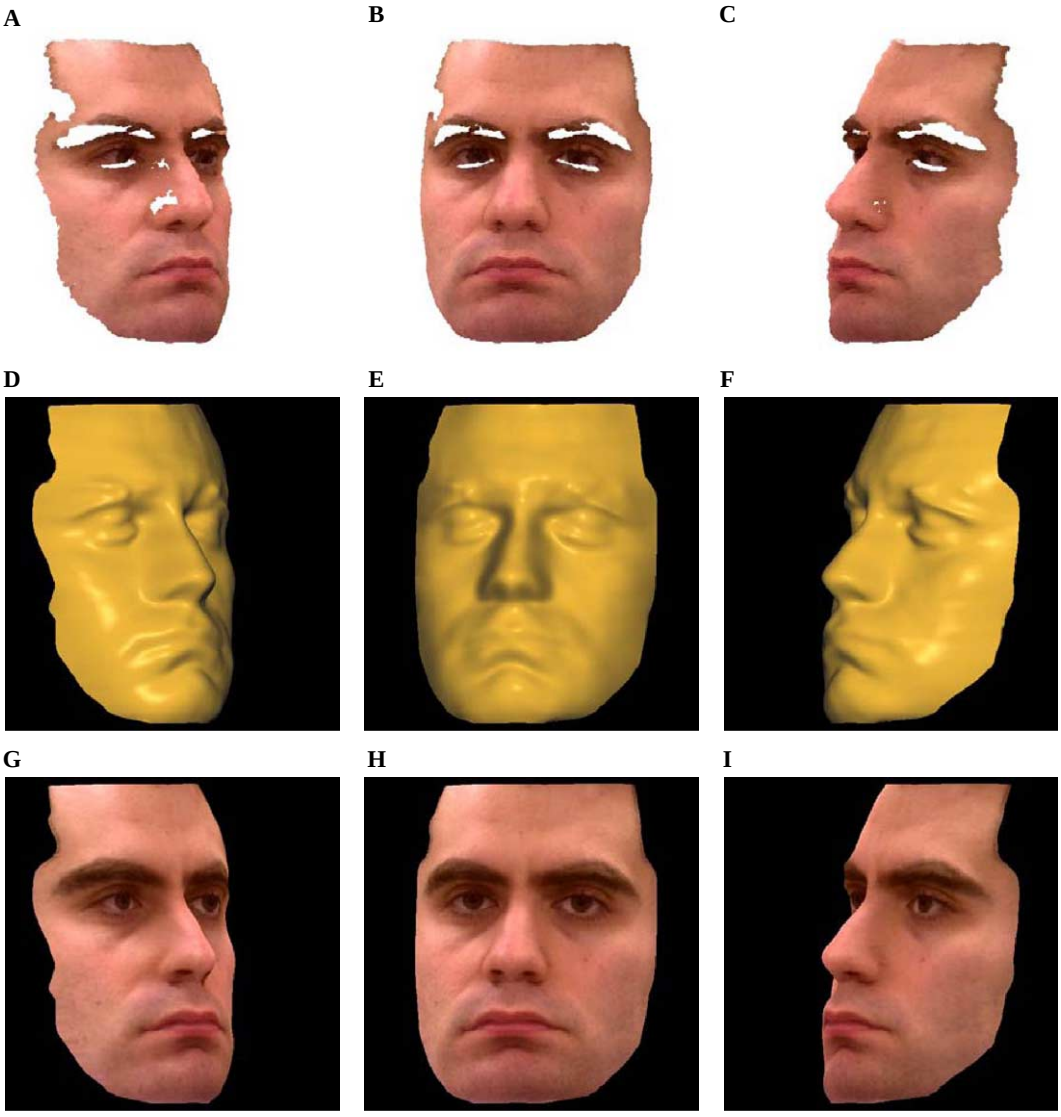

Fig. 25. (A–C) Raw range data obtained from a single camera view. (D–F) Geometry obtained after hole-filling in the image space and B-spline surface fitting. (G–I) Texture-mapped surface reconstructing the face. The subject closed his eyes when the laser passed over his eyes. The texture captured in the first frame when the subject's eyes were open was mapped to the reconstructed face. The images in (D–F), therefore, show the geometry of the face when the subject's eyes were closed.

changed, scene points not visible in an earlier scan become visible. Fig. 16 shows the model face that was placed between the front and back frames. The range data set shown in Figs. 17A–C was obtained by sweeping the laser from the left side. The range data set shown in Figs. 17D–F was obtained by sweeping the laser from the right side. As can be observed, gaps are obtained in areas where the laser is not visible to the camera due to self occlusion. The size of such gaps depends on the position of the laser, the position of the camera, and the geometry of the object. The accuracy of captured range data depends on the triangulation angle or the angle between the laser plane and the camera's optical axis. The larger this angle, the more accurate the captured data will be, but at the same time there will be more occluded points. This means that there is a trade off between reducing the number and size of gaps and increasing the accuracy of captured data. Integrating the data sets captured from the two different views of the laser projector the data set shown in Figs. 18G–I was obtained.

Filling in gaps in the integrated range data set by the weighted mean method described in Section 3.2.6, the range data set shown in Figs. 18A–C was obtained. Since this data set was obtained from a single camera view, hole-filling was performed in the image space. Fig. 18B shows the model face as it appears in the camera view. When the estimated range values are mapped into 3-D, some gaps still appear in the model in places where the object surface makes a large angle with the image plane. When the combined data set is viewed from the side as shown in Figs. 18A and C, small gaps in data can be observed. Such holes are filled by fitting a B-spline surface to the range points as shown in Figs. 18D–F. The figures show a smooth reconstruction of the model face by a

Fig. 26. (A) Image of the actual face. (B) Image of the reconstructed face.

B-spline surface. The reconstructed model after mapping the acquired texture to it is shown in Figs. 18G–I.

In the next example, a Greek statue as shown in Fig. 19 was scanned from two camera views. The scan from the left camera view produced the range data set shown in Figs. 20A–C and the scan from the right camera view produced the range data set shown in Figs. 20D–F. After integrating the two data sets, the combined range data set shown in Figs. 21A–C was obtained. The overlap between the two scans is not large but the scans are large enough to cover the entire front, left, and right sides of the statue. A B-spline surface representation of the integrated data is shown in Figs. 21D–F. As can be observed, the reconstructed surface is smooth and seamless at places where different-view range images overlap. The texture-mapped surface is shown in Figs. 21G–I. Figs. 22A–D show four surround views of the Greek statue at a lower resolution. A range data set was created for each view of the statue. Figs. 23A–C show the range data set obtained by integrating front-left and front-right views. Figs. 23D–F show an integrated range data set obtained from the back-left and the back-right views. The integrated range data set from all four views is shown in Figs. 23G–L. After hole-filling/smoothing and B-spline surface fitting, the geometry shown in Figs. 24A–F was obtained. The reconstructed statue in texture-mapped form is shown in Figs. 24G–L. Compared to the images in Fig. 21 we see that some details on the statue have been lost due to scanning at a lower resolution.

As the last example, a scan of a person's face was obtained. Raw range data acquired from a single front view of the camera are shown in Figs. 25A–C. Near the eyebrows and eyelashes, large gaps in range data are obtained. The dark eyebrows and eyelashes do not reflect sufficient laser light to be detected by the camera. As a result, holes are obtained in captured range data. The geometry obtained after hole-filling and surface fitting is shown in Figs. 25D–F. The face geometry has been reproduced relatively well except near the eyebrows and the eyelashes where missing data at sharply varying surface orientations exist. The reconstructed face in texture-mapped form is shown in Figs. 25G–I. The image of the person's face as seen by the camera and an image of the reconstructed face in the same view are shown in Fig. 26 for comparison.

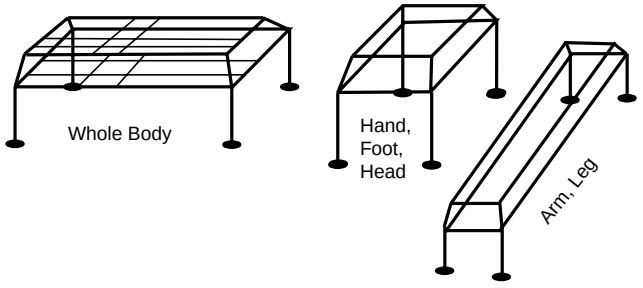

Fig. 27. Reference frames designed for scanning the whole-body; head, foot, or hand; and arm or leg of bed-ridden burn patients. The whole-body double-frame contains adjustable rods that can be moved to create small local double-frames for high-resolution scanning of local areas.

6. Speed

Sparser or denser scans can be obtained by sweeping the laser faster or slower. If a dense scan is required in one area of an object, the laser may be swept slowly or repeated over that area in different directions just like painting over the area with a paintbrush. A scan from a single view of an object as shown in Fig. 18 takes about 15 s. The captured video sequence is processed at a rate of 6 frames/s on an SGI O2 computer with an R10000 processor.

7. Summary and conclusions

The hardware and software organizations of a new hand-held laser range scanner were described. The scanner

uses a reference double-frame to capture multi-view range images and integrate the images automatically. When building the reference double-frame, care should be taken to make sure that the front and back frames are parallel. The distance between the frames determines the resolution in depth. Too small a distance will make the equation of the laser plane inaccurate, while too large a distance will make determination of the intersections of the laser plane with the frames inaccurate due to camera defocus. The distance between the frames should be taken such that markers on the frames and intersections of the laser planes with both frames appear sharp in the captured images. Since our camera was equipped with a zoom lens, we kept the camera relatively far (about 10 feet) from the double-frame but zoomed in the camera to minimize blurring and produce images that showed the object as well as the front and back frames sharp.

The scanner does not require that the laser source and the camera be fixed with respect to each other. The user may hold the laser line generator like a paintbrush and paint over the object to scan it. If desired, the laser source may be translated or rotated automatically using a translation stage or a rotating mirror.

The camera can be freely moved around an object while scanning, producing data from all around the object. When capturing images with a moving camera, care should be taken to include the frame corners in the images. Range data captured from different views of an object will be in the coordinate system of the double-frame and will, therefore, automatically merge to reconstruct the object.

The described scanner allows independent movement of the laser and the camera during a scan. This strength can be a weakness if the additional degree of freedom is not needed. The user has to manually sweep the laser over an object. This at times could be beneficial, enabling scanning of a very complex object from different views, but at times it can be burdensome if the scene is simple and does not require scans from different views. The major contribution of the proposed work is considered to be the development of a reference double-frame that enables automatic calibration and integration of multi-view range images. The double-frame may be custom made to meet different scanning objectives. For instance, the frames shown in Fig. 27 were designed to scan different parts of the body of bed-ridden burn patients.

References

[1] 3D Scanners, <http://www.3dscanners.com/>.

[2] J. Albamont, A. Goshtasby, A range scanner with a virtual laser, Image Vision Comput. 21 (2003) 271–284.

[3] P.J. Besl, Active optical range imaging sensors, Mach. Vision Appl. 1 (1998) 127–152.

[4] P.J. Besl, N.D. McKay, A method for registration of 3-D shapes, IEEE Trans. Pattern Anal. Mach. Intell. 14 (2) (1992) 239–256.

[5] F. Blais, M. Picard, G. Godin, Recursive model optimization using ICP and free moving 3-D data acquisition, in: Proc. of the 4th Internat. Conf. on 3-D Digital Imaging and Modeling, Banff, Alberta, Canada, October 6–10, 2003, pp. 251–258.

[6] J.D. Boissonnat, Geometric structures for three-dimensional shape representation, ACM Trans. Graph. 3 (4) (1984) 266–286.

[7] J.-Y. Bouguet, P. Perona, 3-D photography using shadows in dual-space geometry, Int. Comput. Vision 35 (2) (1999) 129–149.

[8] B. Curless, M. Levoy, A volumetric model for building complex models from range images, Proc. SIGGRAPH (1996) 303–312.

[9] Cyberware four-head whole-body scanner, <http://www.cyberware.com/products/wbinfo.html/>.

[10] Cyberware rotating-head head and face scanner, <http://www.cyberware.com/products/psInfo.html/>.

[11] J. Ferreira, J. Lobo, J. Diasu, Tele-3D—developing a handheld scanner using structured light projection, 3D Data Processing, Visualization Transm. (2002) 788–791.

[12] R.B. Fisher, A.P. Ashbrook, C. Robertson, N. Werghi, A low-cost range finder using a visually located, structured light source, patent pending (9822410.8).

[13] R.B. Fisher, A.W. Fitzgibbon, A. Gionis, M. Wright, D. Eggert, A hand-held optical surface scanner for environmental modeling and virtual reality, Proc. Virtual Reality World (February) (1996).

[14] R. Furukawa, H. Kawasaki, Interactive shape acquisition using marker attached laser projector, in: Proc. of the 4th Internat. Conf. on 3-D Digital Imaging and Modeling, Banff, Alberta, Canada, October 6–10, 2003, pp. 491–498.

[15] K. Gasvik, Moiré techniques by means of digital image processing, Appl. Optics 22 (23) (1983) 3543–3548.

[16] A. Goshtasby, Correction of image deformation from lens distortion using Bézier patches, Comput. Vision Graph. Image Process. 47 (1989) 385–394.

[17] A. Goshtasby, Three-dimensional model construction from multiview range images: survey with new results, Pattern Recogn. 31 (11) (1998) 1705–1714.

[18] A. Goshtasby, S. Nambala, W. deRijk, S. Campbell, A system for digital reconstruction of gypsum dental casts, IEEE Trans. Med. Imaging 16 (5) (1997) 664–674.

[19] P. Hérbert, A self-referenced hand-held range sensor, in: Proc. of the Internat. Conf. 3-D Digital Imaging and Modeling, Quebec City, Canada, May 28–June 1, 2001, pp. 5–12.

[20] A. Hilton, A.J. Stoddart, J. Illingworth, T. Windeatt, Reliable surface reconstruction from multiple range images, 4th European Conf. on Computer Vision, 1996, pp. 117–126.

[21] M. Jackowski, A. Goshtasby, S. Bines, D. Roseman, C. Yu, Correcting the geometry and color of digital images, IEEE Trans. Pattern Anal. Mach. Intell. 19 (10) (1997) 1152–1158.

[22] J. Kofman, G.K. Knopf, Range sensing by an unconstrained and continuously moving laser-scanner without sensor-head pose measurement, in: Proc. of the 2nd Internat. Symp. on Intelligent Manufacturing Systems, August 6–7, 1998, pp. 783–793.

[23] Kreon Technologies, <http://www.kreon3d.com/>.

[24] C.-W. Liao, G. Medioni, Surface approximation of a cloud of 3D points, Graph. Models Image Process. 57 (1) (1995) 67–74.

[25] G.G. Levin, G.N. Vishnyakov, A.A. Naumov, S.S. Abramov, 3-D surface real-time measurement using phase-shifted interference fringe technique for the craniofacial identification, 3-D Image Capture and Applications, Proc. SPIE 3313 (1998).

[26] T. Masuda, Registration and integration of multiple range images by matching signed distance fields for object shape modeling, Comput. Vision Image Understand. 87 (2002) 51–65.

[27] B. McCallum, M. Nixon, B. Price, R. Fright, Hand-held laser scanning in practice, in: Proc. Image and Vision Computing, University of Auckland, New Zealand, 1998, pp. 17–22.

[28] J. Mundy, G. Porter, A three-dimensional sensor based on structured light, in: T. Kanade (Ed.), Three Dimensional Machine Vision, Kluwer Academic Pub., Dordrecht, 1987, pp. 3–61.

[29] D.K. Naidu, R.B. Fisher, A comparative analysis of algorithms for determining the peak position of a stripe to sub-pixel accuracy, Proc. Br. Mach. Vision Conf. (1991) 217–225.

[30] T.K. Ng, T. Kanade, PALM: portable sensor-augmented vision system for large-scene modeling, in: Proc. of the 2nd Internat. Conf. on 3-D Digital Imaging and Modeling, Ottawa, Canada, October 4–8, 1999, pp. 473–482.
[31] Northern Digital, <http://www.ndigital.com/>.
[32] Polhemus, <http://www.polhemus.com/fastscan.htm/>.
[33] V. Popescu, E. Sacks, G. Bahmutov, Interactive point-based modeling from dense color and sparse depth, in: M. Alexa, S. Rusinkiewicz (Eds.), Eurographics Symposium on Point-Based Graphics, 2004.
[34] K. Pulli, Multiview registration for large data sets, in: Proc. of the 2nd Internat. Conf. on 3-D Digital Imaging and Modeling, Ottawa, Canada, October 4–8, 1999, pp. 160–168.
[35] G. Roth, A. Whitehead, Using projective vision to find camera positions in an image sequence, in: Proc. of Vision Interface, Montreal, Canada, 2000, pp. 225–232.
[36] R. Sagawa, K. Ikeuchi, Taking consensus of signed distance field for complementing unobserved surface, in: Proc. of the Internat. Conf. on 3-D Digital Imaging and Modeling, Banff, Alberta, Canada, October 6–10, 2003, pp. 410–417.
[37] B. Sarkar, C.-H. Menq, Smooth-surface approximation and reverse engineering, Comput.-Aided Des. 23 (9) (1991) 623–628.
[38] D. Scharstein, R. Szeliski, A taxonomy and evaluation of dense two-frame stereo correspondence algorithms, Int. J. Conf. Comput. Vision 47 (1/2/3) (2002) 1–35.
[39] W.A. Schulz, Method and apparatus for three-dimensional noncontact shape sensing, U.S. Patent No. RE035816, 1998.
[40] D. Soucy, M. Laurendeau, Multi-resolution surface modeling from multiple range images, IEEE Conf. Comput. Vision Pattern Recogn. (1992) 353–384.
[41] M. Subbarao, G. Surya, Depth from defocus: a spatial domain approach, Int. J. Comput. Vision 13 (1994) 271–294.
[42] R. Szeliski, D. Tonnesen, D. Terzopoulos, Modeling surfaces of arbitrary topology with dynamic particles, Proc. Comput. Vision Pattern Recogn. (1993) 82–87.
[43] M. Takatsuka, G.A.W. West, S. Venkatesh, T.M. Caelli, Low-cost interactive active monocular range finder, Proc. of the 2nd Internat. Conf. on 3-D Digital Imaging and Modeling, Ottawa, Canada, October 1999, pp. 24–33.
[44] E. Trucco, A. Verri, Introductory Techniques for 3-D Computer Vision, Prentice-Hall, New Jersey, 1998, 139–176.
[45] D. Tubić, P. Hébert, D. Laurendeau, A volumetric approach for interactive 3-D modeling, in: Proc. of the 1st Internat. Symp. on 3-D Data Processing Visualization and Transmission, Padova, Italy, June 19–21, 2002, pp. 150–158.
[46] A. Ullrich, N. Studnicka, J. Riegl, Long-range high-performance time-of-flight based 3-D imaging sensors, in: Proc. 1st Internat Symp. on 3-D Data Processing Visualization and Transmission, Padova, Italy, June 19–21, 2002, pp. 852–855.
[47] D. De Vleeschauwer, An intensity-based coarse-to-fine approach to reliably measure binocular disparity, CVGIP: Image Understanding 57 (2) (1993) 204–218.
[48] M. Watanabe, S. Nayar, Rational filters for passive depth from defocus, Int. J. Comput. Vision 23 (3) (1998) 203–225.